1-1-2012

Diffraction of digital micromirror device gratings and its effect on properties of tunable fiber lasers

Xiao Chen

Binbin Yan

Feijun Song

Yiquan Wang

Feng Xiao
Edith Cowan University

See next page for additional authors

10.1364/AO.51.007214
This is an Author's Accepted Manuscript of: Chen, X., Yan, B., Song, F., Wang, Y., Xiao, F. , & Alameh, K. (2012). Diffraction of digital micromirror device gratings and its effect on properties of tunable fiber lasers. Applied Optics, 51(30), 7214-7220. Available here

Diffraction of digital micromirror device gratings and its effect on properties of tunable fiber lasers

Xiao Chen,[1,*] Bin-bin Yan,[2] Fei-jun Song,[1,3] Yi-quan Wang,[1] Feng Xiao,[4] and Kamal Alameh[4]

[1]College of Science, Minzu University of China, Beijing 100081, China

[2]State Key Laboratory of Information Photonics and Optical Communications, Beijing University of Posts and Telecommunications, Beijing 100876, China

[3]China Daheng Group, Inc., #A9 ShangdiXinxi Avenue, Haidian District, Beijing 100085 China

[4]Electron Science Research Institute, Edith Cowan University, Joondalup, WA 6027, Australia

*Corresponding author: xchen@pku.edu.cn

Received 24 April 2012; revised 8 September 2012; accepted 13 September 2012; posted 14 September 2012 (Doc. ID 167366); published 15 October 2012

A digital micromirror device (DMD) is a kind of widely used spatial light modulator. We apply DMD as wavelength selector in tunable fiber lasers. Based on the two-dimensional diffraction theory, the diffraction of DMD and its effect on properties of fiber laser parameters are analyzed in detail. The theoretical results show that the diffraction efficiency is strongly dependent upon the angle of incident light and the pixel spacing of DMD. Compared with the other models of DMDs, the 0.55 in. DMD grating is an approximate blazed state in our configuration, which makes most of the diffracted radiation concentrated into one order. It is therefore a better choice to improve the stability and reliability of tunable fiber laser systems.

OCIS codes: 050.1950, 060.3510.

1. Introduction

Digital light processing (DLP) technology is well known for powering office and classroom projectors, digital cinema solutions, and high-definition televisions. At the heart of DLP technology is the digital micromirror device (DMD), a semiconductor-based array of thousands of individually addressable, tiltable, mirror pixels. These microscopic mirrors are arranged in a rectangular array, which can be individually rotated $\pm 12°$ along the diagonal line, corresponding to an "on" or "off" state during the display [1]. With success of DMDs as the core components used in optical microelectronic mechanical systems and spatial light modulators, a myriad of nonprojector applications are now being enabled by general-use DMDs, including volumetric display, holographic data storage, lithography, scientific instrumentation, and medical imaging [2–6].

Compared with widely used liquid crystal devices (LCDs), DMDs have the advantage in the speed, precision, polarization insensitivity, and broadband capability. Therefore, a new application of DMDs has been attempted to be applied in tunable fiber lasers as wavelength selectors [7]. We have also achieved the use of DMDs to select wavelength and thus construct a DMD-based tunable fiber laser system [8]. The structure is shown in Fig. 1, which mainly consists of an erbium-doped fiber amplifier (EDFA), a 90/10 optical coupler, a polarization controller, a dual fiber collimator, a blazed grating, two lenses, and a DMD. The 90% broadband amplified spontaneous emission (ASE) noise from the EDFA is routed to the DMD through the dual fiber collimator. The ASE is dispersed by the blazed grating with

1559-128X/12/307214-07$15.00/0

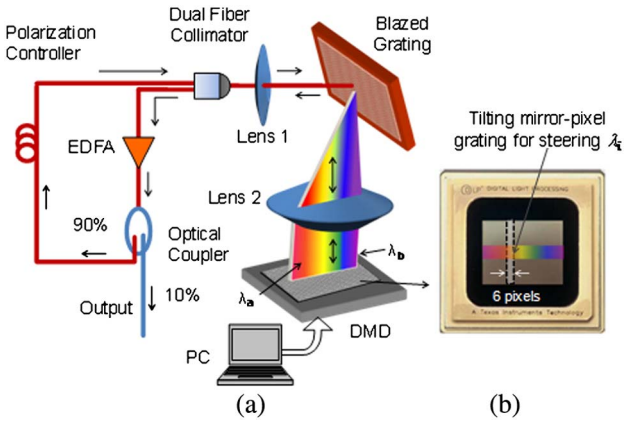

Fig. 1. (Color online) Schematic diagram of the DMD-based tunable fiber laser.

1200/mm in different directions and then illuminates linearly along the active window of the DMD by the lens 2. By driving the appropriate mirror-pixel block to tilt as illustrated in Fig. 1(b), most of the diffracted radiation from the DMD grating is concentrated in a certain order that reflects nearly along the incident path into the collimator, while the others are dropped out with dramatic attenuation. The selected wavebands are amplified by the EDFA, leading, after several recirculations, to high-quality single-mode laser generation. Hence, the fiber laser can be tuned by simply driving the various pixels of the DMD.

Figure 2 is the measured curve of ASE gain noise from an EDFA. The EDFA used in the laser system is a C-band amplifier, having signal gain of 20 dBm and a flatness degree of ±3.5 dB. The EDFA's pump laser is driven by a current of 500 mA. The inset is the measured curve of an arbitrary wavelength selected by the DMD when the optical loop is open. The total insertion loss of the bulk optic component from the input and output ports of a dual fiber collimator was around 11.6 dB, which was mainly due to (1) the lens reflection loss, (2) the blazed grating loss,

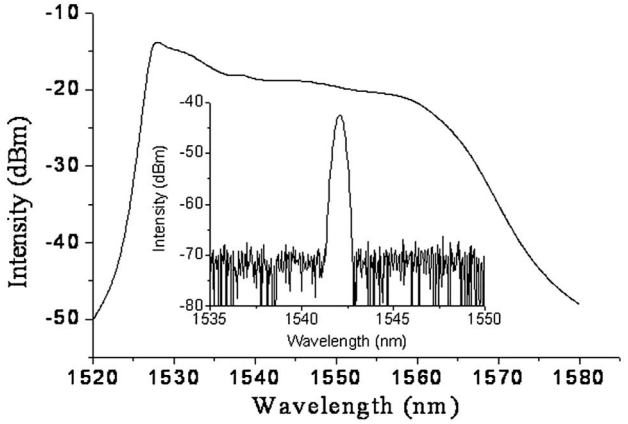

Fig. 2. Measured ASE gain spectrum of a C-band EDFA. The inset is an example of an arbitrary wavelength selected by DMD (optical loop is open).

and (3) diffraction loss and insertion loss of the DMD. Among them, the DMD diffraction loss is the major cause to deteriorate laser signals. As we know, the DMD is actually a two-dimensional "blazed" grating, for which the diffractive behavior in near-infrared wavelengths is evident. For the standard 0.7 in. extended graphics array DMD with pixel pitch 13.68 μm [9], several discrete well-resolved diffractive peaks are observed over a sufficiently large solid angle, which are challenging to couple into the fiber. Therefore, how to maximize the diffraction efficiency and concentrate most of the diffracted energy to the desired order routed into the fiber collimator is important for the stability of the laser output. In the following section, we will analyze the diffractive issue of the DMD and reveal the dependence of diffraction efficiency and pattern on the pixel spacing and the incident angle, so as to reduce the free-space loss and improve the stability of the whole system.

2. Pixel Coding of a DMD

Consider the DMD composed of $(2M+1)\times(2N+1)$ square mirrors with side length δ_0. All mirrors are made to individually rotate ±12° tilt angle along their diagonals once a voltage pulse is applied to the address electrodes under the mirrors. A coordinate system (xyz) is established on the active window of the DMD with the origin at the center of a mirror right in the middle as shown in Fig. 3(a). All mirror pixels are encoded by the location of their center. Meanwhile, a local coordinate system $(\xi\eta\zeta)$ illustrated in Fig. 3(b) is introduced in a mirror P_{mn}. Due to the fill factor of the mirror-pixel area up to 90% for a standard DMD [9] (the fill factor is the ratio of the active reflecting area to the total area of the array of mirrors), the area of a single pixel is approximately equal to the mirror size δ_0^2.

Suppose a monochromatic plane wave illuminating the DMD working region, under the Fraunhofer condition; the diffraction field from differential segment $ds = d\xi d\eta$ (Q) in the mnth pixel [see Fig. 3(b)] is then

$$dA_{mn} = A_0 \exp\{-ik[\Delta''_{mn}(x,y) + \Delta'(\xi,\eta)]\}, \quad (1)$$

where A_0 is the initial amplitude of the wave, $\Delta''_{mn}(x,y)$ is the optical path difference (OPD) between the rays from the center P_{mn} to the origin O, and $\Delta'(\xi,\eta)$ is that from the point Q to P_{mn} within a pixel. Hence, integration of Eq. (1) yields the total electric amplitude A contributed by all pixels in a DMD; that is

$$A = \int dA_{mn} = \sum_{m,n} A_0 e^{-ik\Delta''_{mn}(x,y)} \int_{\sigma_P} e^{-ik\Delta'(\xi,\eta)} d\xi d\eta, \quad (2)$$

where the sum is independent of the integral in the calculation.

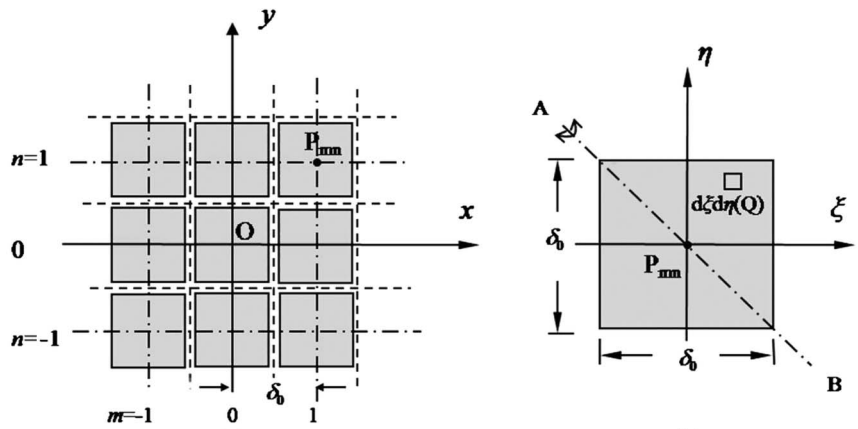

(a) (b)

Fig. 3. (a) Coordinate system (xyz) established on DMD and the pixel coding. (b) Local coordinate system ($\xi\eta\zeta$) introduced in a mirror pixel.

3. Optical Path Difference

A monochromatic plane wave, represented by a pair of rays 1 and 2 inclined at the same angle, arrives at points A and R on a pixel (see Fig. 4). The path difference between the two rays is then

$$\Delta_{AR} = \vec{\nu}_{AR} \cdot \vec{\alpha}, \tag{3}$$

where $\vec{\nu}_{AR}$ is the vector from a point A to R and $\vec{\alpha}$ is the unit vector of incidence.

A. Optical Path Difference Δ' Within a Pixel

In Fig. 5, the unit vector of an incident ray $\vec{\alpha}$ and the corresponding diffraction ray $\vec{\alpha}'$ are defined as follows:

$$\left.\begin{array}{l} \vec{\alpha} = (a, b, c) \\ \vec{\alpha}' = (a', b', c') \end{array}\right\}. \tag{4}$$

Select an arbitrary point $Q(\xi, \eta, \zeta)$ on a mirror, and the path difference between the rays along $\vec{\alpha}$ and $\vec{\alpha}'$ at points P and Q can be determined by dropping two perpendicular lines from Q onto $\vec{\alpha}$ and $\vec{\alpha}'$ at G and G', respectively (see Fig. 5). This path difference is given by

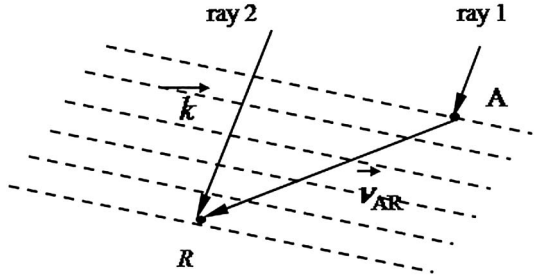

Fig. 4. Diagram of the OPD.

$$\begin{aligned} \Delta' &= (\overline{PG'}) + (\overline{PG}) = (\xi, \eta, \zeta) \cdot \vec{\alpha}' + (-\xi, -\eta, -\zeta) \cdot \vec{\alpha} \\ &= (\xi, \eta, \zeta)(\vec{\alpha}' - \vec{\alpha}) = \xi(a' - a) + \eta(b' - b) + \zeta(c' - c). \end{aligned} \tag{5}$$

The plane equation of a tilting mirror by rotating ψ angle along its diagonal is

$$\zeta = \frac{\tan\psi}{\sqrt{2}}(\xi + \eta). \tag{6}$$

Substituting Eq. (6) into Eq. (5), thus

$$\begin{aligned} \Delta' = \xi\left[(a' - a) + \frac{\tan\psi}{\sqrt{2}}(c' - c)\right] \\ + \eta\left[(b' - b) + \frac{\tan\psi}{\sqrt{2}}(c' - c)\right]. \end{aligned} \tag{7}$$

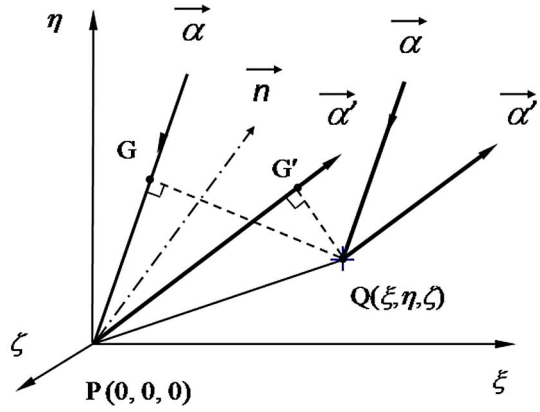

Fig. 5. OPD between the rays along $\vec{\alpha}$ and $\vec{\alpha}'$ at points P and Q in a pixel.

B. Optical Path Difference Δ''_{mn} from the mnth Pixel Center P_{mn} to the Origin O

The position of the mnth mirror is

$$P_{mn} = \delta_0(m, n, 0), \tag{8}$$

where $m = -M, -M+1, \cdots M; n = -N, -N+1, \cdots N$. Referring to Eq. (5), the path difference Δ''_{mn} between the rays along $\vec{\alpha}$ and $\vec{\alpha}'$ at P_{mn} and the origin O is then

$$\begin{aligned}\Delta''_{mn} &= (m\delta_0, n\delta_0, 0)\cdot(\vec{\alpha}' - \vec{\alpha}) \\ &= \delta_0[m(a'-a) + n(b'-b)].\end{aligned} \tag{9}$$

Substituting Eqs. (7) and (9) into Eq. (2), the dependence of the diffraction pattern on $\vec{\alpha}'$ can be determined if the incident wave $\vec{\alpha}$ is given.

4. Single-Pixel Diffraction

The DMD is actually a two-dimensional ordered reflection phase grating. The diffraction contribution of a mirror pixel is similar to that of a slit in the one-dimensional multiple-slit diffraction grating. When we integrate Eq. (2), we neglect the effect of small tilting angle on the domain of integration and approximately obtain the single-pixel diffraction of a DMD, that is

$$\begin{aligned}A' &= \int_{-\delta_0/2}^{\delta_0/2} e^{-ik\left[(a'-a)+\frac{\tan\psi}{\sqrt{2}}(c'-c)\right]\xi} \mathrm{d}\xi \\ &\quad\times \int_{-\delta_0/2}^{\delta_0/2} e^{-ik\left[(b'-b)+\frac{\tan\psi}{\sqrt{2}}(c'-c)\right]\eta} \mathrm{d}\eta \\ &= \delta_0^2 \,\mathrm{sinc}\left\{\frac{\pi\delta_0}{\lambda}\left[(a'-a)+\frac{\tan\psi}{\sqrt{2}}(c'-c)\right]\right\} \\ &\quad\times \mathrm{sinc}\left\{\frac{\pi\delta_0}{\lambda}\left[(b'-b)+\frac{\tan\psi}{\sqrt{2}}(c'-c)\right]\right\}.\end{aligned} \tag{10}$$

To simplify the appearance of things, let

$$\left.\begin{aligned}u' &= \tfrac{\pi\delta_0}{\lambda}\left[(a'-a)+\tfrac{\tan\psi}{\sqrt{2}}(c'-c)\right] \\ u'' &= \tfrac{\pi\delta_0}{\lambda}\left[(b'-b)+\tfrac{\tan\psi}{\sqrt{2}}(c'-c)\right]\end{aligned}\right\}. \tag{11}$$

Therefore, the corresponding flux-density distribution is given by neglecting the constants.

$$I' = |A'|^2 = \delta_0^4 \,\mathrm{sinc}^2 u' \cdot \mathrm{sinc}^2 u''. \tag{12}$$

To analyze the diffraction pattern, it is convenient to transfer a rectangular coordinate into a polar coordinate system. Thus, the component of incident light is rewritten to be

$$\left.\begin{aligned}a &= \sin\theta_0\cos\phi_0, b = \sin\theta_0\sin\phi_0, c = \cos\theta_0 \\ a' &= \sin\theta\cos\phi, b' = \sin\theta\sin\phi, c' = \cos\theta\end{aligned}\right\}, \tag{13}$$

where θ_0 and ϕ_0 are the angles between $\vec{\alpha}$ with ζ and ξ axis, respectively. θ and ϕ are those between $\vec{\alpha}'$ with ζ and ξ axis, respectively. Then substituting Eq. (13) into Eq. (11) leads to

$$\left.\begin{aligned}u' &= \tfrac{\pi\delta_0}{\lambda}\left[(\sin\theta\cos\phi - \sin\theta_0\cos\phi_0)+\tfrac{\tan\psi}{\sqrt{2}}(\cos\theta-\cos\theta_0)\right] \\ u'' &= \tfrac{\pi\delta_0}{\lambda}\left[(\sin\theta\sin\phi - \sin\theta_0\sin\phi_0)+\tfrac{\tan\psi}{\sqrt{2}}(\cos\theta-\cos\theta_0)\right]\end{aligned}\right\}. \tag{14}$$

5. Multiple-Pixel Interference

Substituting Eq. (9) into Eq. (2), the sum of the diffraction contribution from all mirrors is

$$\begin{aligned}A'' &= \sum_{m=-M}^{M}\sum_{n=-N}^{N} e^{-ik\delta_0[m(a'-a)+n(b'-b)]} = \sum_{m=-M}^{M} e^{-ik\delta_0 m(a'-a)} \sum_{n=-N}^{N} e^{-ik\delta_0 n(b'-b)} \\ &= e^{i\frac{\pi\delta_0}{\lambda}[(a'-a)+(b'-b)]} \frac{\sin\left[\frac{\pi\delta_0}{\lambda}(2M)(a'-a)\right]}{\sin\left[\frac{\pi\delta_0}{\lambda}(a'-a)\right]} \frac{\sin\left[\frac{\pi\delta_0}{\lambda}(2N)(b'-b)\right]}{\sin\left[\frac{\pi\delta_0}{\lambda}(b'-b)\right]}.\end{aligned} \tag{15}$$

So the flux-density distribution is

$$I'' = |A''|^2 = \frac{\sin^2[(2M)\nu']\sin^2[(2N)\nu'']}{\sin^2\nu'\sin^2\nu''}, \tag{16}$$

where

$$v' = \frac{\pi\delta_0}{\lambda}(a' - a), \qquad v'' = \frac{\pi\delta_0}{\lambda}(b' - b). \tag{17}$$

In the polar coordinate, Eq. (17) is rewritten in the form

$$\begin{aligned} v' &= \frac{\pi\delta_0}{\lambda}(\sin\theta\cos\phi - \sin\theta_0\cos\phi_0), \\ v'' &= \frac{\pi\delta_0}{\lambda}(\sin\theta\sin\phi - \sin\theta_0\sin\phi_0). \end{aligned} \tag{18}$$

According to the grating equation, the irradiance maximum should satisfy the following condition; that is

$$\left.\begin{aligned} v' &= \tfrac{\pi\delta_0}{\lambda}(\sin\theta\cos\phi - \sin\theta_0\cos\phi_0) = p\pi \\ v'' &= \tfrac{\pi\delta_0}{\lambda}(\sin\theta\sin\phi - \sin\theta_0\sin\phi_0) = q\pi \end{aligned}\right\} \tag{19}$$

with $p, q = 0, \pm1, \pm2, \cdots$. The (p,q)th-order irradiance maximum is labeled as I''_{pq} in short.

We define two parameters $g_p(\theta_0, \phi_0)$, $h_q(\theta_0, \phi_0)$ as follows:

$$\left.\begin{aligned} \sin\theta\cos\phi &= \tfrac{p\lambda}{\delta_0} + \sin\theta_0\cos\phi_0 = g_p(\theta_0, \phi_0) \\ \sin\theta\sin\phi &= \tfrac{q\lambda}{\delta_0} + \sin\theta_0\sin\phi_0 = h_q(\theta_0, \phi_0) \end{aligned}\right\} \tag{20}$$

or the equivalent form is

$$\tan\phi = \frac{h_q(\theta_0, \phi_0)}{g_p(\theta_0, \phi_0)} = \frac{q\lambda/\delta_0 + \sin\theta_0\sin\phi_0}{p\lambda/\delta_0 + \sin\theta_0\cos\phi_0}. \tag{21}$$

According to Eqs. (20) and (21), if the incidence (θ_0, ϕ_0) is provided, the resultant diffraction $(\theta, \phi)_{pq}$ of I''_{pq} can be determined.

$$\left.\begin{aligned} \phi_{pq}(\theta_0, \phi_0) &= \tan^{-1}\left[\frac{h_q(\theta_0,\phi_0)}{g_p(\theta_0,\phi_0)}\right] \\ \theta_{pq}(\theta_0, \phi_0) &= \sin^{-1}\left\{\frac{g_p(\theta_0,\phi_0)}{\cos[\phi_{pq}(\theta_0,\phi_0)]}\right\} \end{aligned}\right\}. \tag{22}$$

6. Discussion

Based on the theory above, we take two standard DMDs as an example to analyze the diffraction issue. The incident wavelength is 1550 nm used in the calculation.

(1) A 0.7 in. DMD composed of (1024 × 768) pixels with the mirror pitch $\delta_0 = 13.68$ μm.

For simplicity, suppose the wave is incident vertically upon the tilting mirror in the angle-bisecting plane in the first octant, namely $\theta_0 = 168°$, $\phi_0 = 45°$. Figure 6 is shown the resultant diffraction distribution. Two sharp irradiance-maximum peaks are observed at $\theta = 6.5°$ and 15.8°, with the multiple-pixel interference peaks modulated by the single-pixel diffraction.

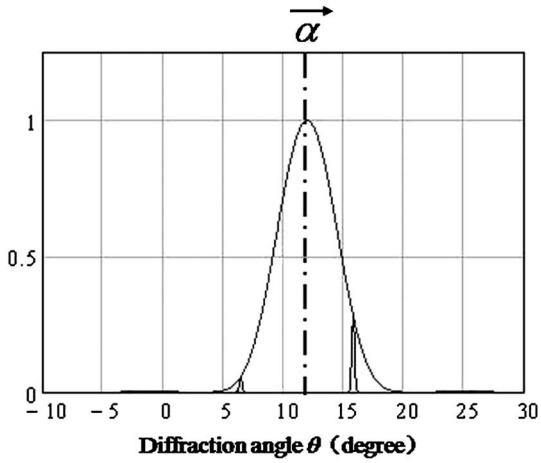

Fig. 6. Diffraction distribution of light radiating on a 0.7″ DMD with the wave incident vertically upon the tilting mirror in the angle-bisecting plane in the first octant (red curve for single-pixel diffraction, blue curve for multiple-pixel interference).

Furthermore, in the tunable fiber laser shown in Fig. 1, the irradiance maximum of diffraction should be confined within the aperture of the lens 1; thus it is possibly coupled into the fiber ring cavity to form the laser. Therefore, the constraint condition is expressed as follows:

$$\vec{\alpha}_{p,q} \cdot (-\vec{\alpha}) > \cos(\Delta\theta), \tag{23}$$

where $\vec{\alpha}$ is the unit vector of incidence and $\vec{\alpha}_{p,q}$ is that of (p,q)-order diffraction irradiance maximum. $\Delta\theta = \tan^{-1}(12.7/75) \approx 9.7°$ (12.7 and 75 mm are the aperture radius and focal length of the lens 1, respectively).

Table 1 gives the entire irradiance maxima over a sufficiently large solid angle and the corresponding diffraction angle (θ/ϕ) and relative intensity $I(\theta, \phi)$ of each (p/q)-order irradiance maximum. The results show that there are only four irradiance maxima left, which satisfy both the constraint condition and intensity requirement. They all distribute in symmetry of the bisection plane. Those peaks in intensity less than 0.03 or those that do not satisfy the constraint condition are neglected. Furthermore, in order to prove the validity of the theoretical model, we use an infrared fluorescence card to detect the diffraction

Table 1. Irradiance Maxima of Light in 1550 nm Radiating on a 0.7″ DMD Over a Large Solid Angle

p/q	−4	−3	−2	−1
−4	—	21.2/212.2	18.4/194.6	—
	—	(0.022)	(0.015)	—
−3	21.2/237.8	15.8/225	12.0/202.4	11.3/170.1
	(0.022)	0.279	0.148	(0.021)
−2	18.4/255.4	12.0/247.6	6.5/225	—
	(0.015)	0.148	0.055	—
−1	—	−11.3/99.9	—	—
	—	(0.021)	—	—

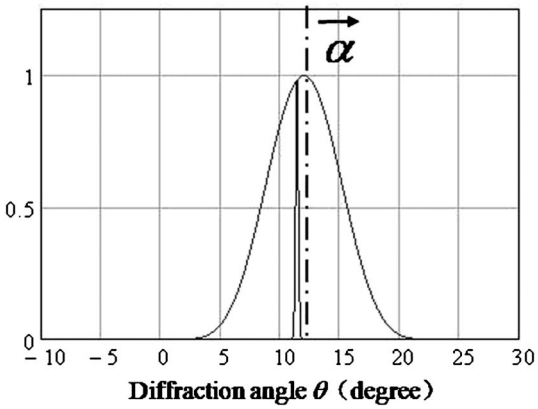

Fig. 7. Diffractive distribution of light radiating on a 0.55″DMD on the bisecting plane.

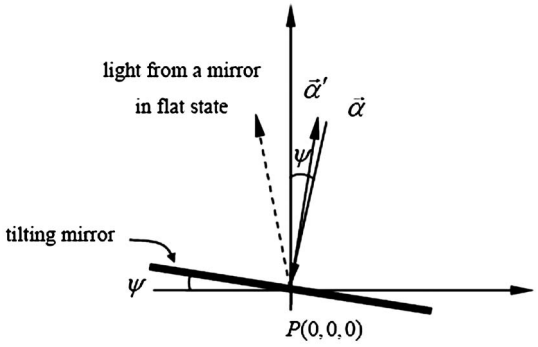

Fig. 8. Optimal experimental configuration of light radiating on a DMD system.

irradiance maxima by illuminating a 0.7″DMD with light in 1550 nm wavelength. There are really four discrete well-resolved diffractive peaks observed over a large solid angle, which is quite in agreement of the theory. However, in the fiber laser system, only the brightest order of diffractive light $I_{(-3,-3)} \approx 0.279$ is adjusted to reflect nearly along the incident path, while the other peaks with about 70% energy are dropped out. Hence, a 0.7″DMD as a component used in the fiber laser system deteriorates the stability of the system.

(2) A 0.55″ DMD composed of (1024 × 768) pixels with the mirror pitch $\delta_0 = 10.8$ μm. The wave with wavelength 1550 nm is also incident at the position $\theta_0 = 168°$, $\phi_0 = 45°$.

For a 0.55″ DMD, there is only one peak of the irradiance maximum within the envelope curve of single-pixel diffraction, as illustrated in Fig. 7. Due to the peak of multiple-pixel interference close to the single-pixel maximum, that is, approximately the blazed grating condition, most of the diffracted radiation is concentrated in one order, so that the relative intensity $I_{(-2,-2)}$ is about 0.98, approaching 1. In the experiment, if the light is incident at the angle $\theta_0 = 168°$, as shown in Fig. 8, the diffractive peak from the tilting mirror is proved to reflect nearly along the incident path. Meanwhile, the light reflected from the flat mirror cannot be coupled into the

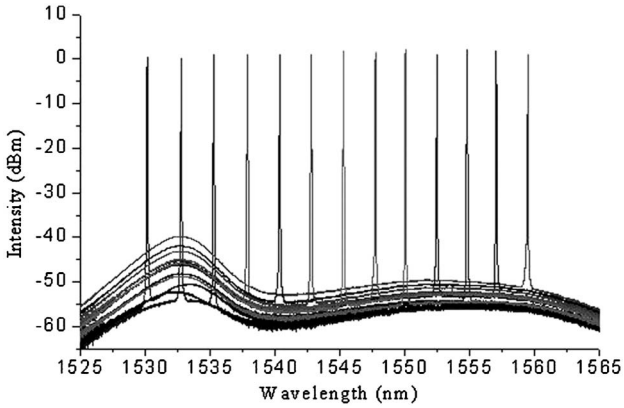

Fig. 9. Measured output intensities of the DMD-based fiber laser with the wavelength tuning over C-band.

ring cavity. Thus, by driving some block of mirrors to tile, we can select the wavelength reflected from the corresponding tilting mirrors into the fiber ring, so that these selected wavebands are amplified by the EDFA, leading, after several recirculations, to high-quality single-mode laser generation. Figure 9 shows the experimental results of laser output based on a 0.55″ DMD. The laser tuning range is 1530–1560 nm with the tuning resolution 0.08 nm. The FWHM of a lasing line is about 20 pm, and the side mode suppression ratio (SMSR) is greater than 50 dB. Therefore, a 0.55″ DMD is proved to be a good choice to improve the stability and reliability of the laser system.

7. Concluding Remarks

DMD as a spatial light modulator has been widely used in many areas. Compared with LCD, DMD has the advantage in the speed, precision, polarization insensitivity, and broadband capability. We successfully employed DMD as a wavelength selector in tunable fiber lasers and studied the dependence of diffraction properties of this kind of a two-dimensional DMD grating on the incident angle and pixel spacing. The diffraction orders and intensity distribution of DMDs in 0.7 and 0.55 in. size with different pixel spacing are discussed in detail. The diffraction of a 0.7″ DMD is a little far away from the blazed grating condition as the energy is distributed in four diffractive peaks, resulting in low efficiency. For a 0.55″ DMD, however, most of the diffracted radiation is concentrated into one order in the approximate blazed state, which is therefore a better choice as a wavelength tuner to improve the stability and reliability of the laser system.

We appreciate very much the technical support from Texas Instruments. This work is supported by the National Science Foundation of China (11204387), the Key Project of Science and Technology from Ministry of Education of China (212205), the “985 Project” (Grant No. 98507-010009, 98504-012004), and the “211 Project” of the Ministry of Education of China.

References

1. D. Dudley, W. Duncan, and J. Slaughter, "Emerging digital micromirror device (DMD) applications," Proc. SPIE **4985**, 14–20 (2003).
2. Y. Lim, H. Joonku, and L. Byoungho, "Phase-conjugate holographic lithography based on micromirror array recording," Appl. Opt. **50**, H68–H74 (2011).
3. M. L. Huebschman and H. R. Munjuluri Garner, "Dynamic holographic 3-D image projection," Opt. Express **11**, 437–445 (2003).
4. P. M. Friedman, G. R. Skover, G. Payonk, A. N. B. Kauvar, and R. G. Geronemus, "3D in-vivo optical skin imaging for topographical quantitative assessment of non-ablative laser technology," Dermatol. Surg. **28**, 199–204 (2002).
5. S. D. Cha, P. C. Lin, L. J. Zhu, P. C. Sun, and Y. Fainman, "Nontranslational three-dimensional profilometry by chromatic confocal microscopy with dynamically configurable micromirror scanning," Appl. Opt. **39**, 2605–2613 (2000).
6. T. Fukano and A. Miyawaki, "Whole-field fluorescence microscope with digital micromirror device: imaging of biological samples," Appl. Opt. **42**, 4119–4124 (2003).
7. W. Shin, B.-A. Yu, Y. L. Lee, T. J. Yu, T. JoongEom, Y.-C. Noh, J. Lee, and D.-K. Ko, "Tunable *Q*-switched erbium-doped fiber laser based on digital micro-mirror array," Opt. Express **14**, 5356–5364 (2006).
8. X. Chen, Y. Q. Wang, K. Z. Huang, F. J. Song, G. X. Chen, Z. Z. Sang, B. B. Yan, Y. Zhang, F. Xiao, and K. Alameh, "Tunable polarization-maintaining single-mode fiber laser based on a MEMS processor," *CLEO: QELS-Fundamental Science*, OSA Technical Digest (Optical Society of America, 2012), paper JW2A.59.
9. http://www.ti.com/analog/docs/memsmidmodlevel.tsp?sectionId=651&tabId=2447.